Multi-mode energy management method of integrated photovoltaic energy storage system

A. Zhichong Shao[1], B. Yuxuan Bi[2], C. Bin Liang[3], D. Houji Li[4] and E. Yong Wang[5]

[1] *Dept.of Electrical Engineering, Shanghai Jiaotong University, China, szc20001114@sjtu.edu.cn*
[2] *Dept.of Electrical Engineering, Shanghai Jiaotong University, China, biyuxuan@sjtu.edu.cn*
[3] *Dept.of Electrical Engineering, Shanghai Jiaotong University, China, Bingo_524@sjtu.edu.cn*
[4] *Dept.of Electrical Engineering, Shanghai Jiaotong University, China, lihoushen@sjtu.edu.cn*
[5] *Dept.of Electrical Engineering, Shanghai Jiaotong University, China, wangyong75@sjtu.edu.cn*

***Abstract*-- This paper presents a single-phase power conversion system (PCS) consisting of photovoltaic part, battery storage part and inverter part. The topology contains a full-bridge LLC converter and a bidirectional buck-boost for storage interface, a boost converter for PV interface and a HERIC inverter for grid interface. This article innovatively designs three modes to handle different kinds of operating state. Mode1 and Mode3 corresponds to the off-grid state while Mode2 corresponds to the on-grid state. The droop control method in the storage interface, a double closed loop control method in the invertor interface and a voltage loop control method in the PV interface are adopted in this system respectively. Multi-mode energy management has significant advantages in high efficiency and reliability. An experimental prototype of this system is built to verify the feasibility of the system structure and mode switching strategy.**

***Index Terms*-- energy management, photovoltaic generation, Power converter, renewable energy generation**

I. INTRODUCTION

Nowadays, in order to achieve carbon neutrality, the photovoltaic industry has grown tremendously. But the photovoltaic power generation is unstable and might cause fluctuations in the power grid, so the storage battery part is added. The storage side plays a role in absorbing and releasing the photovoltaic energy, reducing the energy exchange with the grid. This system usually supplies power to the nearby off-grid loads, acting as a self-sufficient microgrid.

A typical topology of this system contains a full-bridge LLC converter, a bidirectional buck-boost, a boost converter and the Highly Efficient and Reliable Inverter Concept (HERIC) inverter which is connected to grid.

There are numerous researches on topology design, control strategy and application. A control method combining the droop control and the virtual synchronous generator is proposed to achieve accurate tracking of the active power reference under on-grid mode and off-grid mode [1]. The HERIC inverter is used in the last stage of the power conversion system (PCS), improving the efficiency and reliability of the entire three-stage system [2]. A cascaded H-bridge PCS is proposed, in which the power control method can be achieved flexibly and the SOC balance can work with a low harmonic current [3]. New algorithms such as genetic algorithm (GA) are raised to minimizing the peak current and expanding the zero-voltage switching (ZVS) range [4].

A new topology of the DC-DC part, namely the CLLLC resonant circuit is raised to simplify the topology and to improve efficiency by soft switching and bidirectional adjustable gain. The operational principles, voltage-gain characteristics, and design procedure of the CLLLC resonant converter are analyzed and discussed and the maximum conversion efficiency is up to 96.5 % [5]. A detailed derivation of the CLLLC principle, voltage gain and parameter design, as well as the design of a PFM control method in the case of grid imbalance is given in order to handle complicated circumstance. [6]

This photovoltaic energy storage system is widely used in the new energy applications. A 500kW solar power based microgrid system for space applications is proposed [7] and the photovoltaic power is used to supply the household off-grid load [8].

However, only one set of control strategy is not enough to handle with different operating conditions, such as PV power exceeding the load demand, PV power not enough for the load demand, the grid fault and so on. Therefore, the research on the mode switching is necessary. This article designs three modes to deal with different operating state. The detailed mode operating situation can be seen in Fig.1-3. Finally, the feasibility and effectiveness of the proposed control method is verified by simulation and experimental results.

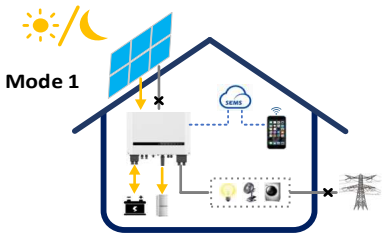

Fig.1 Mode1

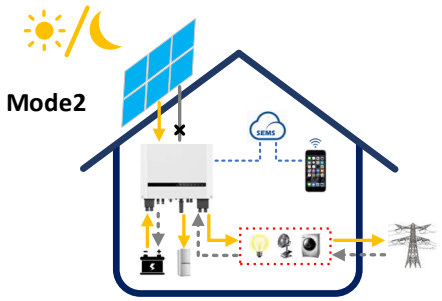

Fig.2 Mode2

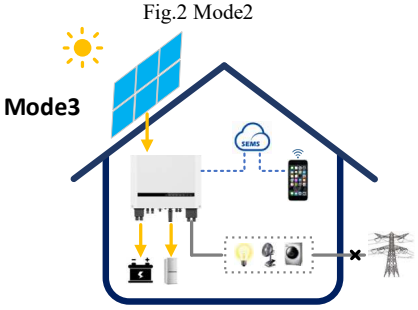

Fig.3 Mode3

II. SYSTEM TOPOLOGY

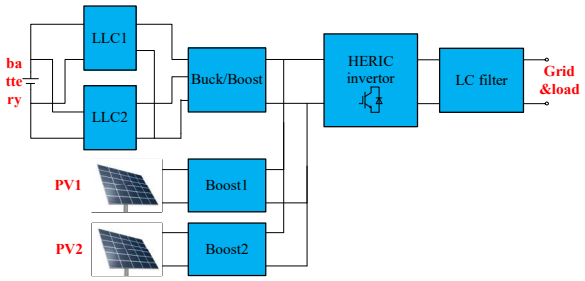

Fig.4 Topology of the whole PCS

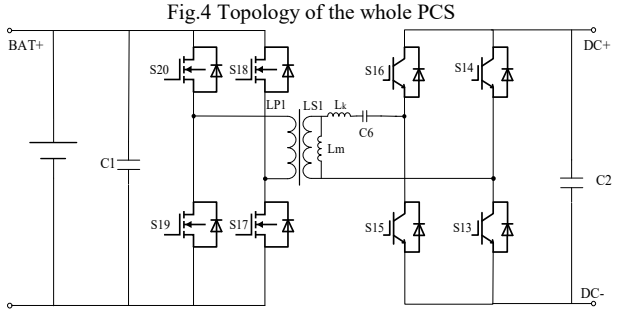

Fig.5 Topology of the LLC circuit

As is shown in Fig. 4, on the energy storage side, a 48V storage battery is connected in parallel to two LLC converters, in which the transformer ratio is 6. Then the buck-boost circuit raise the DC voltage up to 400V and the HERIC inverter converts DC power to AC power. The AC output is connected to the grid or to the AC load after the LC filter circuit. The photovoltaic part consists of two photovoltaic panels directly connected to the input of the two boost circuits. The output side is directly connected to the DC side of the HERIC. The detailed topology of the LLC part, the buck-boost part and the heric part are shown below in Fig.5-Fig.7.

The full-bridge LLC converter can realize the bidirectional flow of energy between the battery and the grid. In Fig.5 it can be seen that the parallel inductor is the transformer excitation inductor, and the series inductor is the transformer leakage inductor. It is both capable of zero-voltage switching and zero-current switching. Thereby, this topology is completely soft switching [9]. To be precise, when the operating frequency is higher than the resonant frequency, the resonant cavity is in an over-resonant state, at which time the primary switching tube achieves ZVS and the secondary diode has turn-off losses. When the operating frequency is lower than the resonant frequency, the resonant cavity is in an under-resonant state, the primary switching tube achieves ZVS and the secondary diode has no off losses and achieves ZCS.

The buck-boost converter is adopted to raise the 300V voltage on the medium voltage DC side to the 400V rated voltage of the DC bus. The high-voltage DC bus voltage can be stabilized by this converter. Current of the inductor is detected by Hall sensors to realize the DC-bus voltage and input current double closed-loop control and improve the dynamic performance of the system.

The HERIC topology is adopted in this PCS. The topology is shown in Fig. 7. On the basis of full bridge invertor, two power electronic switches operating at the grid frequency and isolating the PCS from the grid is added in the HERIC converter. These two additional IGBTs operating at the grid frequency have functions that isolating the PCS from the grid, and preventing the reactive power exchange between the filter inductors and capacitor during the zero-voltage state. Leakage current is usually hard to reduce for inverters, which poses a safety threat to human and it increases the harmonic content of the grid current. Leakage current of HERIC inverter is greatly reduced in this PCS so that saves all the trouble above.

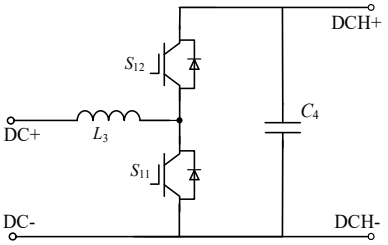

Fig.6 Buck-Boost converter

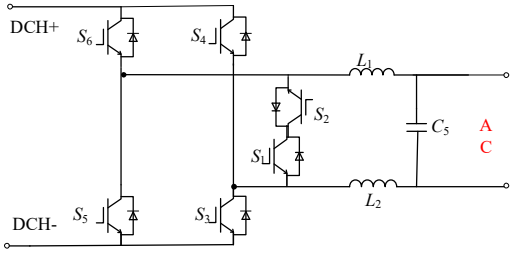

Fig. 7 Heric invertor

III. CONTROL STRATEGY OF DIFFERENT MODES

A. Mode1&3

Mode 1&3 are working modes in off-grid state. Mode1 corresponds to the situation when the PV power is less than the sum of the maximum charging power on the storage side and the power required by the off-grid load. Mode3 corresponds to the situation when the PV power is more than the sum of those two.

The DC bus voltage is controlled by the storage interface converter with droop control in Mode1 while it is controlled by the photovoltaic interface converter with a voltage control loop in Mode3. The photovoltaic interface converter will operate with MPPT in Mode1. The ac voltage is controlled by the Heric inverter. The detailed control diagrams are as shown in Fig. 8 and Fig. 9.

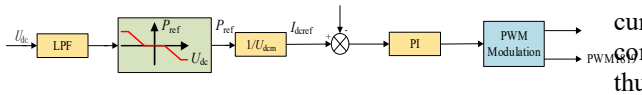

Fig.8 Control diagram of the storage side converter in Mode 1&3.

A droop relationship between the DC bus voltage U_{dc} and the power from the battery side P_{ref} is constructed in Mode1. A dead band is added, which means when U_{dc} is in a range (390 V~410V), there is no power exchange between the storage side and the DC bus, otherwise the storage side will supply power for the DC bus when U_{dc} gets lower and will draw power from the DC bus when U_{dc} gets higher in order to keep U_{dc} stable. The advantage of the droop control with a dead band is that it avoids frequent direction switching of the LLC while maintaining U_{dc} stable.

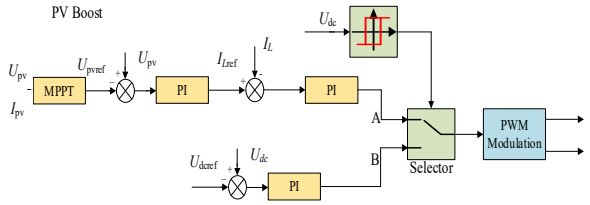

Fig.9 Control diagram of the PV boost

When the DC bus voltage is low, it means the power on the PV side does not exceed the sum of the maximum charging power on the storage side and the load power, so the MPPT control scheme is adopted on the PV side to ensure the maximum power output on the PV side, which corresponds to the switch connected to the A side in Fig.9.

When the PV power exceeds the sum of maximum charging power and load power, DC bus voltage will rise constantly up to 600V, which can cause damage to the electrolytic capacitors, power electronic switches and other devices on the DC bus. Mode3 is designed to solve this problem. If U_{dc} is detected more than 450V, the PV boost convertor will work in constant voltage mode and U_{dcref} will be set as 450V. A hysteresis is introduced to ensure if DC bus voltage is lower than 425V Mode3 turns to Mode1.

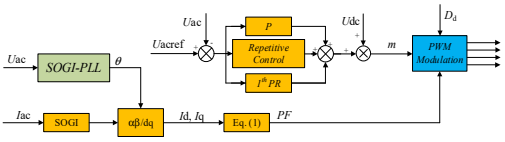

Fig.10 Control diagram of the inverter

The control strategy of the inverter under the off-grid circumstance can be seen in Fig.10. The inverter controls output voltage of the AC side. This requires information of the load-side power factor angle which is given in PF and a controller with PI + Repetitive Control is selected to achieve constant voltage control. This PI and Repetitive Control combines the advantages of the two controllers. The repeat controller is mainly used when the grid current is unchanged. Compared to PI control, the system will obtain better steady- state accuracy of current. When the current command of grid changes suddenly, the PI controller is mainly used to dynamically track the current, thus ensuring the rapid dynamic response of the system.

B. Mode2

Mode 2 is a working mode in on-grid state. The overall control strategy of Mode2 is shown in Fig.11.

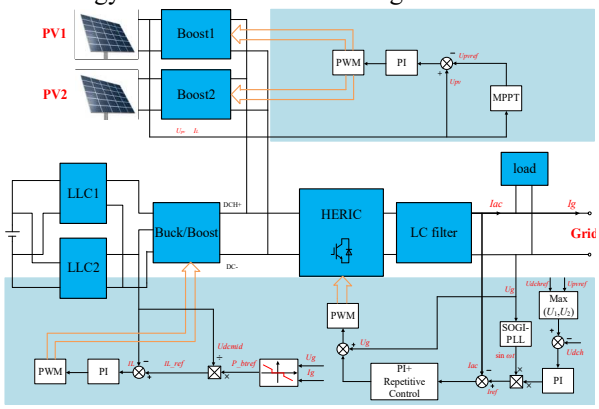

Fig.11 overall control strategy of Mode2

The PV interface converter works with MPPT scheme, when the PV generated power is greater or less than the power required by the load, the DC bus charges or discharges the battery in order to control the active power of the grid side current port to 0. When the PV voltage is too high, the PV interface converter stops operation and the inverter switches the voltage loop to the MPPT output voltage to stabilize the DC bus voltage while maximize the PV output. The detailed control diagrams are shown below.

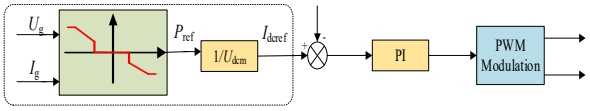

Fig.12 storage side converter in on-grid working mode

A droop relationship between grid side power U_g*I_g and the power from battery side P_{ref} is constructed. As can be seen from Fig.12, it uses the nearly same method as in Mode1 while its effect is to prevent power exchange between off-grid side and grid side. The difference

between Mode2 droop control and Mode1 droop control is that in Mode1 the droop relation is between U_{dc} and P_{ref} while in Mode2 the droop control relation is between U_g*I_g and P_{ref}. When $U_g*I_g>0$, the battery supply power to load and When $U_g*I_g<0$, the battery extract power to charge itself. That is the most economical way to operate.

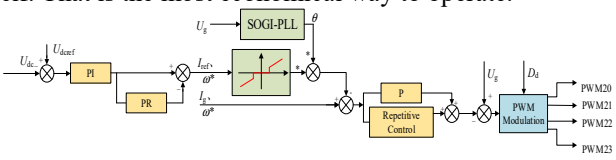

Fig.13 Double closed-loop control method of the inverter

A double closed-loop of U_{dc} and I_g is used to keep the DC bus voltage stable. When the system is connected to grid, it follows that,

$$U_{dc} \propto P_g = U_g \cdot I_g = U_{gm} I_{gm} \sin(\omega t)\sin(\omega t + \theta) \quad (1)$$

That means U_{dc} has the second order harmonic component. In order to get a DC I_{ref}, a PR controller is adopted to eliminate the second order harmonic component. The transfer function of the PR is:

$$G_{PR}(s) = K_p + \frac{K_r \cdot s}{s^2 + \omega_0^2} \quad (2)$$

This controller extracts the second order harmonic component and eliminate it with the original output. Then I_{ref} gets into a dead band to avoid frequent direction switching. A repetitive controller is adopted to suppress the harmonics of the grid current and improve the accuracy of the steady-state control.

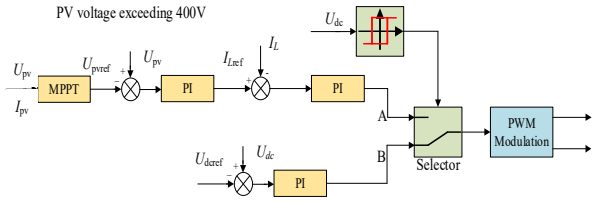

Fig.14 Control diagram of the PV voltage over 400V

As can be seen in Fig.14, since there is almost no potential difference between the voltages on both sides of the PV interface converter when the PV panel voltage exceeds 400V, the duty cycle of the Boost circuit is automatically reduced to near 0 by the voltage-current loop, which is equivalent to a straight-through at both ends of the converter. Therefore, there is no need to make changes to the MPPT of the PV interface converter and the voltage-current loop behind it. Instead, no operations such as setting the controller to zero or switching the algorithm are performed after the voltage calculated by the MPPT exceeds 400 V. This prevents the system from experiencing violent voltage fluctuations after the power and voltage on the PV side have changed.

IV. MODE SWITCHING

Switching between Mode1 and Mode3 is explained in the above.

The converter performs island detection in Mode 2, and actively detects whether the converter is in islanding operation and switches to off-grid operation in case of grid failure. In off-grid operation, the grid-side voltage is also sampled, and the converter can return to Mode 2 when the grid is restored. Switching from Mode2 to Mode1&3 are as follows.

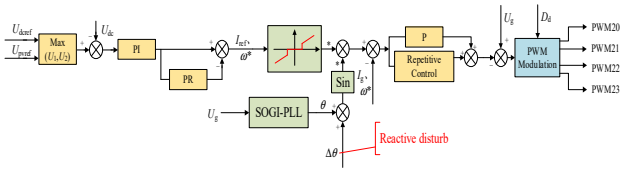

Fig.15 Island detecting in Mode2

By observing whether the injected reactive disturbance makes the frequency of the grid-side voltage fluctuate significantly, the converter can be judged whether it enters islanding state. If so, it will turn to off-grid operation. When the converter is in normal grid-connected state, as the reactive power disturbance required for islanding detection is very small, the output current waveform of the converter will not be significantly distorted, which ensures the network-side power quality in steady state. The reactive power disturbance during active detection is generally controlled within 5%, and the corresponding disturbance power factor angle $\Delta\theta$ is calculated to be less than 2.86°

V. SIMULATION AND EXPERIMENTAL RESULTS

A. Simulation waveform

The simulation results are shown below.

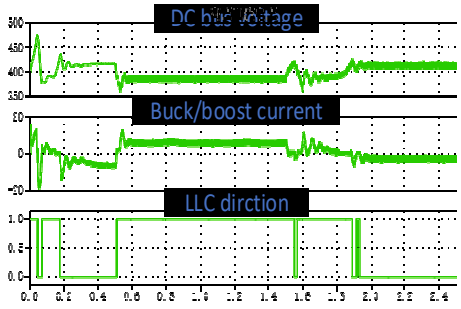

Fig.16 Mode1 switching LLC direction

As can be seen in Fig.16, the off-grid load power switches from 500W initially to 4 kW at 0.5 s and the PV power rises from 2.5 kW to 5.0 kW at 1.5 s. According to the off-grid droop control strategy, the energy storage side absorbs the excess PV power before 0.5 s and charge the storage battery. At 0.5s, after the load on the grid side exceeds the PV input power, the energy storage converter switches the power transfer direction to output power so as to keep the DC bus voltage stable around 400V. Finally, at 1.5s, after the PV input power increases and exceeds load power, the storage side converter switches the power direction again and the batteries are charged.

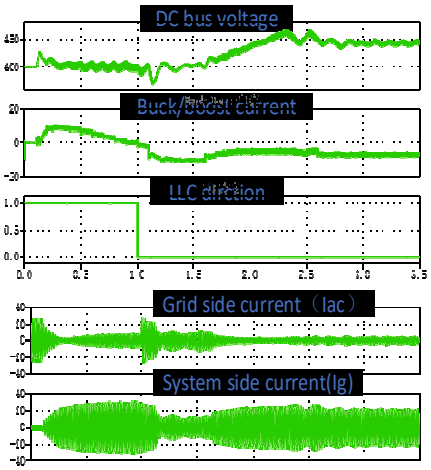

Fig.17 Mode2 PV voltage more than 400V

Fig.17 shows that at 1.0 second, the sunshine suddenly becomes strong and the MPPT reference voltage of PV is higher than the bus reference voltage(400V). At this time, the reference voltage of the inverter is changed to the output voltage of the MPPT of the PV panel and the LLC direction is switched. The power output of the PV panel charges the battery as well as supplying the load. As can be seen from Fig.17, the grid side current has always been small and that shows the control strategy of the inverter suppresses the power exchange between the system side and the grid side. The grid side current and the system side current represent I_{ac} and I_g according to Fig.11.

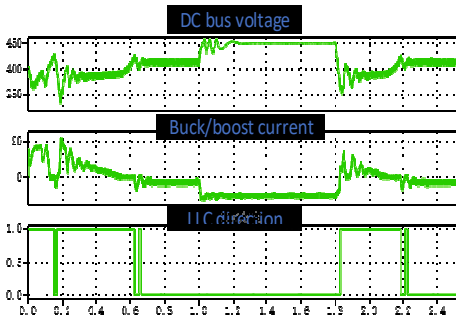

Fig.18 Mode3&1 switching

It can be seen from Fig.18 that at 1.0s, the grid side load switches from a heavy load of 4kW to a light load of 500W and the load switches back to 4kW at 1.8s. The maximum power of the PV is always 5kW, then according to the analysis of the previous control algorithm, the converter should be in mode 1 operation before 1.0s. And when the load is lightened, as the maximum power of the PV is greater than the sum of the maximum chargeable power of the storage battery and the power of the load, the converter automatically switches to mode 3 operation, and the PV converter controls the DC bus voltage. And at 1.8s, after the load is aggravated again, the converter switches to mode 1 again and the PV interface converter continues with the MPPT strategy.

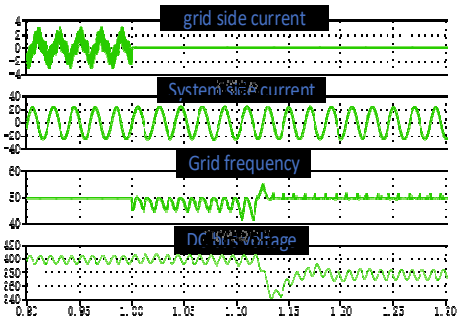

Fig.19 off-grid switching

The grid operates normally until 1.0s when grid is suddenly disconnected. At the same time the island detection is carried out at 1.1s and the system can be switched to off-grid operation at 1.12s. As can be seen in Fig.19, after the injection of reactive power disturbances, the frequency of the network side voltage fluctuates significantly, indicating that the converter is in islanding mode and the converter are switched to off-grid operation. Meanwhile, during normal grid-connected operation, the reactive disturbance required for islanding detection is minimal and does not cause significant distortions in the output current waveform of the converter, thus ensuring the grid side power quality.

B. Experimental waveform

Table.1: experiment parameter

Battery	Rated Voltage(V)	48
	Maximal Current(A)	100
PV	MPPT range (V)	125~550
	Maximal power(W)	6000
Grid	Rated AC voltage (V)	230
	Maximal AC current (A)	22.8
	Maximal power (VA)	5000

Table.1 shows the experimental parameter of the system and Fig.20-22 displays the waveforms of the PV panel voltage（U_{pv}）;AC current of the inverter output (I_{AC}) and it should be emphasized that I_{AC} means the current of the load, either on-grid load or off grid load so that I_{AC} should not be zero in mode 1 or mode 3 since I_{AC} does not represent the grid current; the buck-boost current of the storage side (I_{LLC}) and the DC bus voltage (U_{dc}) during mode switching. The rated DC bus voltage is 400V.

From Fig.20 to Fig.22, it can be seen that the power output of the inverter in steady state is almost constant when switching between Mode 1 and Mode 2. When off-grid, the power of the load is constant, so the excess energy charges the bus capacitor voltage. After the bus voltage rises to near 450V, the system enters Mode 3. When the PV power drops to less than the sum of the load side and battery charging power, the bus capacitor discharges and the bus voltage drops. When the bus voltage drops below 425V, mode 3 turns into mode 1. That explains in Fig.21, U_{pv} and U_{dc} drops. While the power of the load is constant, load side current I_{AC} increases when the U_{dc} drops.

According to droop relationship between U_{dc} and the power from battery, I_{LLC} increases when the U_{dc} droops. That explains each waveform change in Fig.21 and the similar explanation can be applied in Fig.22.

It is now possible to achieve continuous full-mode free switching of the prototype at rated voltage, with no obvious overshoot or abnormalities in the switching process, and energy storage side can also be switched forward and backward normally according to the different modes.

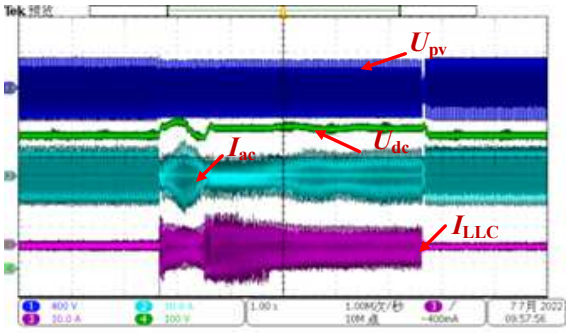

Fig.20: Mode1-2-1

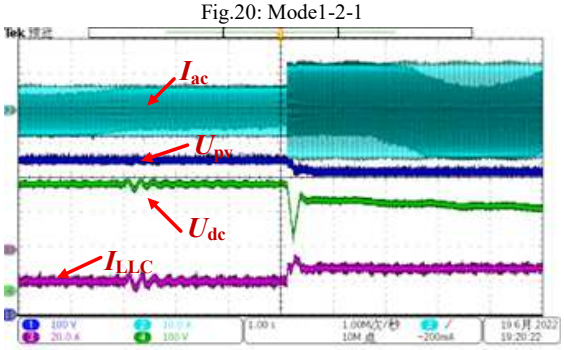

Fig.21:Mode3-1

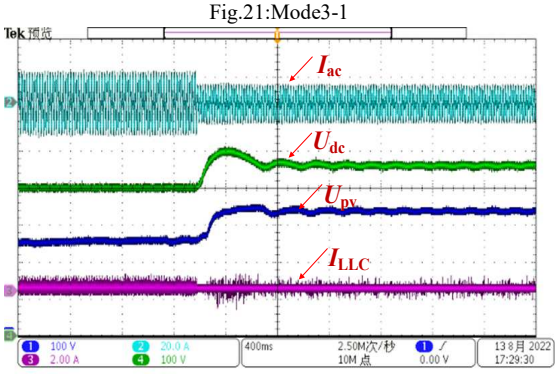

Fig.22:Mode2-3

C. *Efficiency*

The full range of power conversion efficiencies from 5kW to -5kW were tested, in which discharging the battery is the positive direction and charging the battery is the negative direction. It can be seen from table.2 that the conversion efficiency of the system can be maintained above 90% over the entire range, with peak efficiencies of over 95%. From light load to full load, the efficiency rises and then falls and the efficiency of the charging mode is slightly higher than that of the discharging mode.

Table.2: mode1&3 efficiency

DC power(W)	Load power(W)	efficiency
955.44	901.59	94.36%
1903.48	1803.18	94.73%
2900.84	2704.77	93.24%
3903.68	3606.36	92.38%
4961.32	4507.95	90.86%
-827.48	-872.794	94.81%
-1676.88	-1761.19	95.21%
-2487.92	-2662.78	93.43%
-3637.34	-3920.39	92.78%
-4467.32	-4899.99	91.17%

Last, the physical picture of the 6kW single-phase power conversion system is shown in Fig.23

Fig.23: 6kW single-phase power conversion system

VI. CONCLUSION

In view of the instability of photovoltaic power generation, this paper constructs an integrated photovoltaic storage system, in which a multi-mode energy management method is adopted. The working conditions for different modes and the condition required for mode switching are shown in Fig.24. Considering the complexity of operating conditions, this paper constructs three operation modes and realizes efficient management of energy by switching between operation modes. Finally, the effectiveness and feasibility of the proposed method is verified by simulation results and experiments by building a 6kW experimental platform.

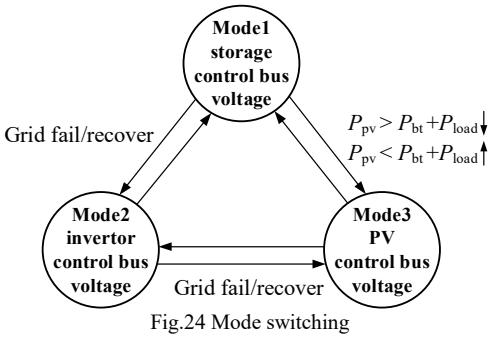

Fig.24 Mode switching

REFERENCES

[1] X. Meng, J. Liu and Z. Liu, "A generalized droop control for grid-supporting inverter based on comparison between traditional droop control and virtual synchronous generator control", *IEEE Trans. Power Electronics.*, vol. 34, no. 6, pp. 5416-5438, 2019, doi: 10.1109/TPEL.2018.2868722.

[2] Y. Lv, Z. Peng and Y. Wang, "Design of A Novel 2.5kW Energy Storage Bidirectional Power Conversion System," *2021 IEEE 12th Energy Conversion Congress & Exposition - Asia (ECCE-Asia)*, 2021, pp. 2022-2027, doi: 10.1109/ECCE-Asia49820.2021.9479232.

[3] G. Hai-Feng, C. Man, C. Yang, M. Qin-Dong and L. Zhi-Bin, "Design of 2MW/10kV cascaded H-bridge power conversion system," *2014 International Conference on Power System Technology*, Chengdu, 2014, pp. 3335-3340, doi: 10.1109/POWERCON.2014.6993906.

[4] L. Jiang, L. Gong, X. Jin, Z. Shao and W. Yong, "Multi-objective Optimization for Dual Active Bridge Converter Based on Genetic Algorithm," *2022 International Power Electronics Conference (IPEC-Himeji 2022- ECCE Asia)*, Himeji, Japan, 2022, pp. 2444-2450, doi: 10.23919/IPEC-Himeji2022-ECCE53331.2022.9807139.

[5] H. -T. Chang, T. -J. Liang and W. -C. Yang, "Design and Implementation of Bidirectional DC-DC CLLLC Resonant Converter," *2018 IEEE Energy Conversion Congress and Exposition (ECCE)*, Portland, OR, USA, 2018, pp. 2712-2719, doi: 10.1109/ECCE.2018.8557697.

[6] J. Kong *et al*., "A Control Strategy of CLLLC DC Transformers under Unbalanced AC Voltage Conditions in Hybrid Microgrids," *2021 IEEE 5th Conference on Energy Internet and Energy System Integration (EI2)*, Taiyuan, China, 2021, pp. 611-616, doi: 10.1109/EI252483.2021.9713333.

[7] M. D'Antonio, C. Shi, B. Wu and A. Khaligh, "Design and Optimization of a Solar Power Conversion System for Space Applications," *IEEE Trans. Ind. Appl.*, vol. 55, no. 3, pp. 2310-2319, May-June 2019, doi: 10.1109/TIA.2019.2891228

[8] C. Zhang and Z. Hao, "An isolated household grid-connected photovoltaic power system," *2017 IEEE International Electric Machines and Drives Conference (IEMDC)*, 2017, pp. 1-7, doi: 10.1109/IEMDC.2017.8002191.

[9] W. Chen, P. Rong and Z. Lu, "Snubberless Bidirectional DC–DC Converter With New CLLC Resonant Tank Featuring Minimized Switching Loss," *IEEE Trans. Ind. Electron.*, vol. 57, no. 9, pp.3075, doi: 10.1109/TIE.2009.2037099